

NRC Publications Archive Archives des publications du CNRC

Modelling and analysis of hydrodynamics of a submerged structure in extreme waves using a SPH-based tool

Islam, Mohammed; Seo, Dong Cheol; Raman-Nair, Wayne

This publication could be one of several versions: author's original, accepted manuscript or the publisher's version. / La version de cette publication peut être l'une des suivantes : la version prépublication de l'auteur, la version acceptée du manuscrit ou la version de l'éditeur.

For the publisher's version, please access the DOI link below. / Pour consulter la version de l'éditeur, utilisez le lien DOI ci-dessous.

Publisher's version / Version de l'éditeur:

<https://doi.org/10.1115/OMAE2021-63034>

ASME 2021 40th International Conference on Ocean, Offshore and Arctic Engineering. Volume 6. Ocean Engineering, 2021-10-11

NRC Publications Archive Record / Notice des Archives des publications du CNRC :

<https://nrc-publications.canada.ca/eng/view/object/?id=ef55d83c-e526-4a09-be57-340c01237b91>

<https://publications-cnrc.canada.ca/fra/voir/objet/?id=ef55d83c-e526-4a09-be57-340c01237b91>

Access and use of this website and the material on it are subject to the Terms and Conditions set forth at

<https://nrc-publications.canada.ca/eng/copyright>

READ THESE TERMS AND CONDITIONS CAREFULLY BEFORE USING THIS WEBSITE.

L'accès à ce site Web et l'utilisation de son contenu sont assujettis aux conditions présentées dans le site

<https://publications-cnrc.canada.ca/fra/droits>

LISEZ CES CONDITIONS ATTENTIVEMENT AVANT D'UTILISER CE SITE WEB.

Questions? Contact the NRC Publications Archive team at

PublicationsArchive-ArchivesPublications@nrc-cnrc.gc.ca. If you wish to email the authors directly, please see the first page of the publication for their contact information.

Vous avez des questions? Nous pouvons vous aider. Pour communiquer directement avec un auteur, consultez la première page de la revue dans laquelle son article a été publié afin de trouver ses coordonnées. Si vous n'arrivez pas à les repérer, communiquez avec nous à PublicationsArchive-ArchivesPublications@nrc-cnrc.gc.ca.

OMAE2021-63034

MODELLING AND ANALYSIS OF HYDRODYNAMICS OF A SUBMERGED STRUCTURE IN EXTREME WAVES USING A SPH-BASED TOOL

Mohammed Islam

Ocean Coastal and River
Engineering Research Centre,
National Research Council
Canada Here
St. John's, NL

Dong Cheol Seo

Ocean Coastal and River
Engineering Research Centre,
National Research Council
Canada Here
St. John's, NL

Wayne Raman-Nair

Ocean Coastal and River
Engineering Research Centre,
National Research Council
Canada Here
St. John's, NL

ABSTRACT

The applications of a Smoothed Particle Hydrodynamics (SPH)-based, a Finite Volume Method (FVM)-based and a Boundary Element Method (BEM)-based tools to investigate the nonlinear interactions between large waves and a submerged horizontal circular structure and to some extent a rectangular cylinder at various submergence depths in deep water conditions are presented. The main aim is to validate the Lagrangian technique based SPH tool to predict the wave-structure interaction forces under large waves.

The features of typical force curves in a wave cycle, the magnitude of wave forces, and the influence of relative axis depth of the structure in deep water conditions are investigated, primarily using an open-sourced SPH tool. Simulations were carried out in 2D with one deepwater wave at multiple submergence depths. The water surface elevations are predicted at different near- and far-field locations. The time-averaged mean and the average amplitude of the horizontal and vertical forces acting on the cylindrical model at various submergence depths are plotted and then physically interpreted. The wave forces and surface elevations are compared with the available published experimental studies and CFD (both FVM and BEM) predictions. Good agreement between the SPH predictions and the measurements was obtained for the submerged body's surface elevation and hydrodynamic forces at all submergence depths. The FVM tends to overestimate the wave forces compared to the SPH predictions and the measurements, particularly for the shallowly submerged structure when extreme wave breaking occurs. The BEM predictions are reasonable for the non-wave breaking cases.

Keywords: SPH, FVM, Hydrodynamics, wave-structure interactions, numerical simulations; Simple offshore structure.

1. INTRODUCTION

The study of the interaction between partially or fully submerged bodies and surface waves, regardless of water depth, is of long-standing interest to many subsea, offshore and coastal engineering applications, namely submerged breakwaters, horizontal pontoons of semi-submersibles and tension-legged platforms (TLP), Submarines, Submerged Floating Tunnel (SFT), wave energy devices (WED), etc. Surface-piercing bodies in the presence of large waves become exposed to extreme forces originated by severe free surface wave motions. On the other hand, completely submerged bodies may produce desirable reflective and dissipative properties with less demanding structural designs. The wave loads on a structure become less as the submergence depth increases and disappear at a submergence depth known as the so-called "wave base" (Moonasun et al., 2016) [1]. Even the largest storm waves may go unnoticed if a structure or a submarine are submerged to a reasonable depth. Floating bridges and floating oil rigs are constructed so that most of their mass is below the wave base to be unaffected by wave motion. Offshore floating airport runways have been designed using similar principles (Moonasun et al., 2016) [1]. The research of submerged bodies in water waves thus received considerable attention for the last several decades.

The interaction between a submerged cylinder and linear and nonlinear surface waves has been studied using analytical and potential theory-based methods, numerically using traditional CFD methods and experimentally by many authors. The great variety of available good-quality studies makes it a good choice for testing novel numerical codes and experimental techniques. The remaining of this section presents a comprehensive literature survey of various models and measurement techniques dedicated to predicting the wave loads on submerged offshore structures.

The core of the work that addressed the above issues has been almost all based on analytical and potential flow theory. Dean (1948) [2] proposed a linear solution to the diffraction problem of monochromatic waves over a submerged horizontal circular cylinder and found that the reflection coefficient is zero under the deep water condition. Ursell (1950) [3] confirmed this conclusion by applying a multipole expansion method, which was more reasonable for computation. Ogilvie et al. (1963) [4] firstly computed the first-order wave force and the second-order mean drift force on the horizontal cylinder by extending Ursell's (1950) [3] method. Ursell (1950) [3] and Ogilvie (1963) [4] also investigated the wave radiation problem for a circular cylinder in forced oscillations and showed that it is possible to absorb all the power in a sinusoidal wave by forcing a cylinder to move in a circular path. Vada (1987) [5] applied an integral equation method to develop a second-order frequency-domain model and computed the first and second harmonics of the wave forces on a submerged circular cylinder. Wu (1993) [6] formulated a mathematical model to calculate the forces exerted on a submerged cylinder undergoing large-amplitude motions. Skotner et al. (1994) [7] proposed a numerical boundary integral equation method combined with a nonlinear time-stepping procedure to calculate wave forces on a large, submerged, horizontal circular cylinder. Teixeira (2010) [8] used a semi-implicit two-step Taylor- Galerkin method to integrate Navier-Stokes equations for investigating the interaction between a regular wave and an immersed horizontal cylinder. The analysis shows that the viscous effects only affect the area that is very close to the cylinder.

More recently, full nonlinear potential-based numerical wave tank (NWT) models have also been used to examine the higher harmonics of wave forces on a horizontal submerged circular cylinder, such as Guerber et al. (2010, 2012) [9] [10], Koh and Cho (2011) [11], Chen (2012) [13] and Bai et al. (2014) [12]. Guerber et al. (2010) [9] extended a two-dimensional fully nonlinear potential wave model to include a submerged horizontal cylinder of arbitrary cross-section. Chen (2012) [13] developed a new vortex-based panel method for calculating a 2-D flow around a hydrofoil submerged under a free surface with energy dissipation. Koh and Cho (2011) [11] proposed a two-dimensional (2D) Fully Nonlinear Potential Flow (FNPF) time-domain simulations for computing the higher-harmonic components of the transmitted wave passing over a submerged circular cylinder to show that it is causing a horizontal negative drift force. Kim et al. (2013) [14] carried out an experimental study on the hydrodynamic behaviours of two submerged concentric cylinders. Bai et al. (2014) [12] used a three-dimensional numerical wave tank model based on higher-order BEM to investigate the interaction between fully nonlinear water waves and fully submerged fixed or moving structures. The 4th-order Runge-Kutta scheme is adopted to update the free water surface boundary conditions expressed in a Lagrangian formulation.

For a deeply submerged horizontal cylinder, the well-known Morison's equation (Morison et al. 1950) [15] has also been widely used in calculating wave loads on a relatively small

structure, which uses coefficients for drag and inertia forces and they depend on Reynold's number, Re , and Kuelegan-Carpenter (K-C) number. This method is not capable of handling the nonlinearity in waves as the structure approaches near the surface. By introducing a varying immersed volume of a cylinder and considering the buoyancy effect, Dixon et al. (1979) [16] modified Morison's equation to calculate the force on a partially submerged horizontal cylinder; however, they found that the modified Morison's equation was inapplicable, and this results in bad agreements between the theoretical forces value and measured ones as the wave height and wave steepness increased.

Owing to the inherent limitations, the potential flow model discussed above cannot produce reasonable hydrodynamic predictions when viscous effects play important roles. Researchers have attempted to overcome this limitation by physical model testing and viscous numerical investigations. Chaplin (1981, 1984a, 1984b, 2001) [17] [18] [19] [20] carried out a series of experimental and numerical studies on non-linear wave interactions with a submerged horizontal circular cylinder. The laboratory tests by Chaplin (1984b) [19] showed that the first harmonics of the wave forces predicted by the potential flow model are significantly overestimated. Based on the experimental observations, the lift force caused by the nonzero circulation and the boundary layer separation due to viscous effects leads to the differences between the experimental measurements and the potential flow solutions. However, the direct support from the flow visualizations was not easy to be obtained in the experiments. Chaplin (1984b) [19] analyzed the influence of the Keulegan-Carpenter number on the harmonics of the applied force. Contento and Codiglia (2001) [21] conducted laboratory tests and measured the wave forces on a submerged horizontal circular cylinder under different submergence at low Keulegan-Carpenter (Kc) numbers. The experimental data showed that the high harmonics of the wave forces have evident dependence on the submergence. Tavassoli and Kim (2001) [22] developed a 2D viscous NWT to simulate the wave forces on a submerged horizontal circular cylinder in the laminar flow regime with a low Reynolds (Re) number. The numerical results showed notable differences in terms of the first harmonics of wave forces and the mean vertical forces with respect to the experimental observations by Chaplin (1984b). The experimental study of Longuet-Higgins (1977) [23] on the mean forces exerted by waves on a submerged horizontal circular cylinder reported the existence of negative mean horizontal forces and suggested the negative mean horizontal forces being attributed to wave breaking. Inoue and Kyojuka (1984) [24] presents physical measurements of nonlinear wave loads acting on submerged cylinders by using fairly large models. Nonlinear effects of the incident wave amplitude, the cylinder submergence and the cross-sectional geometries were studied. Those results were compared with numerical calculations to the second-order. The model overestimated the wave loads when the cylinder was close to the free surfaces as the model was unable to capture the nonlinear effects such as wave breaking. Chaplin (2001) [20] and Schønberg and Chaplin (2003) [25] performed more detailed experimental and

numerical studies of the nonlinear wave interactions with a submerged horizontal cylinder.

Khalil (2001) [26] investigated the wave-induced forces acting on horizontal cylinders submerged beneath water waves with an axis parallel to the wave crests. The author measured the wave-induced drift and vertical forces on circular and rectangular cylinders due to regular sinusoidal waves of length 1.57 and 3.14 m. Each cylindrical model was tested at eight different depths of submergence. The author presented the time-averaged mean horizontal and vertical forces acting on the cylindrical model at various depths of submergence and concluded that the breaking of waves behind a shallowly submerged cylinder is primarily responsible for the generation of nonlinear wave forces. The negative drifting force which acts on a shallowly submerged cylinder is a direct consequence of wave-breaking. This drifting force, however, tends to vanish when the cylinder is deeply submerged. The data presented in Khalil (2001) [26] is the primary validation data source for the current investigation.

In a more recent endeavour, Conde et al. (2009) [27] performed an experimental study in conjunction with numerical analysis to study the fully nonlinear behaviour of a two-dimensional horizontal cylinder in waves. Muellenhof and Slotta (1971) [28] reported the results of a laboratory investigation of the wave-induced forces on a submerged cylinder. Force and pressure distributions on a cylinder located on and near a wave basin floor are correlated with surface water waves of varying amplitude and period. The horizontal and vertical components of forces on the cylinder are registered by strain gauge outputs and by measuring pressure distributions around the cylinder with pressure transducers.

Experiments on the free surface flow around surface piercing or submerged structures are time-consuming and expensive to achieve, requiring appropriate facilities and well-designed experimental studies to minimize the errors. Numerical wave tank (NWT) based on Computational Fluid Dynamics (CFD) tools is often used as an alternative to obtaining the hydrodynamic responses on marine structures. Among the CFD (Computational Fluid Dynamics) models, mesh-based or meshless approaches can be found. Several mesh-based commercial, open-sourced, and in-house developed CFD software has been utilized to model the nonlinear ocean waves (regular and irregular waves) and complex structure interactions, namely Flow-3D and IOWA ANSYS, Star-CCM+ and OpenFOAM. Among the existing meshless methods, Smoothed Particle Hydrodynamics (SPH) (Violeau and Rogers, 2016) [29] is possibly the most popular and has attained the required level of maturity to be used for engineering purposes.

Xiao et al. (2013) [30] investigated the interaction of solitary wave and uniform current and the forces acting on a horizontal cylinder near the free surface using CFD, OpenFOAM package, a method based on the Reynolds-averaged Navier–Stokes (RANS) equations, and the k- ϵ turbulent model the Volume of Fluid (VOF) method. The model is satisfactorily tested against both experimental data of flow forces acting on a horizontal cylinder and the analytical solution of a solitary wave. Modelling

results indicate that forces from combined wave and current action are larger than simple wave force and current force summations. Ottens et al. (2014) [31] simulated waves past a submerged cylinder by using k- ω SST turbulence model combined with a VOF method. Different cases were simulated in different water submerged drafts, wave heights and periods. Comparisons were conducted between the potential theory results, the CFD results and the model test data. Chen et al. (2015) [32] investigated wave forces on partially submerged circular and square cylinders using the Navier–Stokes equation and VOF method spatially discretized using finite elements. Moonasun et al. (2016) [1] evaluated the adequate depth of waves on the submarine at a water depth using the CFD tool, Flow-3D software, based on solving the RANS equations and VOF method. Liu et al. (2017) [33] investigate both regular and irregular waves past a fixed horizontally semi-submerged circular cylinder by solving Navier-Stokes equations discretized by finite volume method (FVM) and using VOF, available in OpenFOAM platform and utilizing waves2Foam (an OpenFOAM based add-on library for wave generations and absorption). Subsequently, the authors investigated the effects of wave height and wavelength on wave-structure interaction.

Teng et al. (2018) [34] carried out numerical simulations for wave action on a submerged horizontal circular cylinder using a viscous fluid model and focused on examining the discrepancies between the viscous fluid results and the potential flow solutions. The authors used the OpenFOAM package to establish the viscous NWT model equipped with a renormalization group (RNG) model for turbulent closure, a volume of fluid (VOF) technique for interface capture, a no-reflection wave generator and a wave-damping function for long-time simulations. The accuracy of the NWT model in predicting large amplitude nonlinear wave propagation and hydrodynamic forces on the structures is validated against available analytical solutions and experimental data. The authors analyzed the relationship between the vortex shedding and the parameters of wave amplitude, Kc number, Re number and wave steepness.

Besides the traditional CFD tools, the meshless Lagrangian method based Smoothed Particle Hydrodynamics (SPH) tool was also used. Aristodemo et al. (2017) [35] adopted a diffusive weakly-compressible SPH model for predicting the horizontal and vertical hydrodynamic forces induced by solitary waves on submerged horizontal circular cylinders and compared the results with laboratory measurements. Experimental and numerical analyses were performed in the inertia-dominated regime where these force components are more relevant than the drag and lift ones. The deviation from the full inertia regime was highlighted in the simulations by the occurrence of a couple of asymmetric vortices behind the cylinder. The excellent agreement between experimental and SPH forces and kinematics at the cylinder has allowed the numerical calibration of the hydrodynamic coefficients in the Morison and transverse semi-empirical equations by different time-domain methods. The authors also proposed simple empirical formulas based on the knowledge of wave amplitude to calculate the hydrodynamic coefficients.

In addition to the investigations on deep water waves, nonlinear shallow-water wave interactions with submerged bodies also received significant attention in the past few decades. However, obtaining a thorough understanding of the wave-body interaction and wave propagation in shallow water presents hydrodynamicists with significant challenges because of the complexity of the governing equations, the nonlinear free-surface boundary conditions, and in some cases, the presence of neighbouring structural members (Zhong and Wang 2009) [36]. Zhong and Wang (2009) [36] introduced a time-accurate stabilized finite-element approximation for the numerical investigation of fully nonlinear shallow-water waves for cases representing the propagation of solitary waves, collisions of two solitary waves, and wave-structure interactions show reasonably good agreement with experimental measurements and other published numerical solutions. The comparisons between results from the present fully nonlinear wave model and weekly nonlinear wave model are presented and discussed.

From the above discussion, we can notice that most previous numerical investigations using potential flow and CFD models mainly focused on studying deeply submerged horizontal circular cylinders or plates in water waves due to the ease of implementation. However, the complex response of a shallowly submerged structure under the action of large nonlinear waves in confined water depth is not well understood. Even in the RANS-based time-domain approach, a volume-discretized method, such as the FEM and FVM, might encounter some unsolvable difficulties in the mesh generation for the highly-deformed computational domain. The SPH-based tools have a high potential to eliminate the meshing issue and model large waves and structure interactions and subsequent flow separations. The authors are not aware of any published results for an SPH-based fully nonlinear study of a submerged structure at multiple depths undergoing actions from large waves in confined water depths.

The present study aims at obtaining a good insight into this problem by using SPH-based numerical simulation. The approach presented here uses a fully nonlinear viscous flow model based on the weakly compressible SPH available in DualSPHysics. The FVM-based commercial RANS solver, Star-CCM+ and an in-house developed BEM-based tool were also used in this study for comparison purposes for a limited number of cases. The overall approach is as follows. First, a brief description of the numerical methods and their implementation is presented in Section 2. After that, Section 3 provides an analysis of the accuracy of the present numerical models based on a comparison with published experimental results of free surface regular waves past a submerged cylinder at different submergence depths in terms of the hydrodynamic forces and free surface elevations. An in-depth discussion on the nonlinear wave-structure interactions between the shallowly submerged cylinder and a discussion on the effects of the submergence depth due to the waves is presented in this section. Section 4 provides a number of concluding remarks on the accuracy and applicability of the SPH, FVM and BEM methods.

2. NUMERICAL METHODS

2.1 Smooth Particle Hydrodynamics (SPH) Method

SPH currently represents one of the most popular meshless Lagrangian particle models (e.g., Violeau and Rogers, 2016) [29]. Over the course of recent decades, has been applied to a broad range of flow processes and fluid-structure interaction problems like sloshing phenomena (e.g., Delorme et al., 2009) [37], water entry of solid bodies (e.g., Sun et al., 2015) [38], flow impacts (e.g., Pugliese Carratelli et al., 2016) [39], environmental problems (Aristodemo et al., 2010) [40], free-surface open channels (Federico et al., 2012) [41] and jets into water bodies (Aristodemo et al., 2015) [42]. In the field of offshore and coastal engineering, SPH, for example, applied to investigate wave propagation (e.g., Dalrymple and Rogers, 2006) [43] and wave generation and absorption (Altomare et al., 2017) [44] processes, and the interaction of regular or irregular waves with structures such as vertical (e.g., Altomare et al., 2015) [45], perforated (Meringolo et al., 2015) [46] and porous (Ren et al., 2014) [47] breakwaters, floating objects (Bouscasse et al., 2013) [48] and wave energy devices (Barreiro et al., 2016) [49], Crespo et al., 2017 [50]). At present, SPH studies involving horizontal circular cylinders refer to their interaction with steady current flows (e.g., Marrone et al., 2013 [51], Bouscasse et al., 2017 [52]).

DualSPHysics is an open-sourced numerical tool based on the Smoothed Particle Hydrodynamics (SPH) method. A complete description of DualSPHysics can be found in [53]. DualSPHysics follow the fundamentals of SPH, which is a Lagrangian and mesh-less method where the fluid is discretized into a set of particles that are nodal points where physical quantities (such as position, velocity, density, pressure) are computed as an interpolation of the values of the neighbouring particles. The contribution of these neighbours is weighted using a kernel function (W) that measures that contribution starting from the initial particle spacing. This distance between particles is normalized using the smoothing length (h), which is the characteristic length that defines the area of influence of the kernel. The kernel presents compact support so that the contribution of particles beyond a cut-off distance (here $2h$) is not considered. The remainder of this section presents a brief description of SPH basics and the governing equations and boundary conditions implemented in DualSPHysics.

2.1.1 SPH Basics

The mathematical fundamentals of SPH are based on integral interpolants. SPH is an interpolation method whereby any function can be expressed using the values of the different properties (velocity, density, pressure) of a set of particles. The basic principle of SPH is to approximate any function $F(\mathbf{r})$ by the discrete integral interpolants using the smoothing kernel function $W(\mathbf{r}, h)$ as follows:

$$F(r_a) \approx \sum_b F(r_b) \frac{\rho_b}{m_b} W(r_a - r_b, h) \quad (1)$$

where ρ_b and m_b are density and mass, respectively, $r_a - r_b$ is the distance between particles, and h determines the maximum distance between interacting particles. The summation is calculated over all the particles b within the region where the kernel is defined. The performance of an SPH model depends heavily on the choice of the smoothing kernel. Kernels are expressed as a function of the non-dimensional distance between particles (q), given by $q=r/h$, where r is the distance between any two given particles a and b , and the parameter h (the smoothing length) controls the size of the area around particle a in which neighbouring particles are considered. Within DualSPHysics, the Quintic [Wendland, 1995] [54] kernel from the Wendland kernel family is often recommended:

$$W(r, h) = \alpha_D \left(1 - \frac{q}{w}\right)^4 (2q + 1) \quad 0 \leq q \leq 2 \quad (2)$$

where, $q = (r_a - r_b)/h$, α_D is equal to $7/4\pi h^2$ in 2D and $21/16\pi h^3$ in 3D. Following the definition of q , the smoothing radius is $2h$.

2.1.2 Governing Formulations

The mass and momentum conservation laws (Navier-Stokes equations) that govern the dynamics of fluid motion are given in Lagrangian form by:

$$\begin{aligned} \frac{D\rho}{Dt} &= -\rho \nabla \cdot \mathbf{v} \\ \frac{D\mathbf{v}}{Dt} &= -\frac{1}{\rho} \nabla p + \nu \nabla^2 \mathbf{v} + \mathbf{g} \end{aligned} \quad (3)$$

where \mathbf{v} is the velocity, t is the time, p is the pressure, ν is the kinematic viscosity, and \mathbf{g} is the gravity. In DualSPHysics, the SPH formulation of the above two equations treats the fluid as weakly compressible, and Tait's equation of state is used to couple the two equations to determine fluid pressure based on particle density (Monaghan, 1994) [55]. Following (Monaghan et al., 1999) [56], the relationship between pressure and density follows the expression:

$$p = \frac{\rho_0 c_0^2}{\gamma} \left[\left(\frac{\rho}{\rho_0} \right)^\gamma - 1 \right] \quad (4)$$

where ρ_0 is the reference density, $c_0 = c(\rho_0) = \sqrt{(\partial p / \partial \rho)}|_{\rho_0}$ is the speed of sound at reference density $\rho_0 = 1000 \text{ kg/m}^3$, p is the pressure, and γ is an empirical constant that depends on the fluid (e.g. $\gamma = 7$ for water). The compressibility is adjusted so that the speed of sound can be artificially lowered; this means that the size of time step taken at any one moment (which is determined according to a Courant condition, based on the currently calculated speed of sound for all particles) can be maintained at a reasonable value. Such adjustment, however, restricts the sound speed to be at least ten times faster than the maximum fluid velocity, keeping density variations to within less than 1%, and therefore not introducing major deviations from an incompressible approach.

Employing the standard SPH interpolation approximation (Monaghan, 2012 and Liu and Liu, 2010) [58] to discretize the conservation equations and incorporating the laminar viscous

stresses and Sub-Particle Scale (SPS) to represent the effects of turbulence lead to the SPH forms of the Navier-stokes equations:

$$\begin{aligned} \frac{D\rho_a}{Dt} &= \sum_b m_b (v_a - v_b) \cdot \nabla_a W_{ab} \\ &\quad + 2\delta h c_0 \sum_b m_b \left(\frac{\rho_a}{\rho_b} - 1 \right) \frac{r_{ab}}{r_{ab}^2 + \eta^2} \\ &\quad \cdot \nabla_a W_{ab} \end{aligned} \quad (5)$$

$$\begin{aligned} \frac{D\mathbf{v}_a}{Dt} &= - \sum_b m_b \left(\frac{p_a}{\rho_a^2} + \frac{p_b}{\rho_b^2} \right) \nabla_a W_{ab} \\ &\quad + \sum_b m_b \left(\frac{4\nu \mathbf{r}_{ab} \cdot \nabla_a W_{ab}}{(\rho_a + \rho_b)(r_{ab}^2 + \eta^2)} \right) \mathbf{v}_{ab} \\ &\quad + \sum_b m_b \left(\frac{\tau_a}{\rho_a^2} + \frac{\tau_b}{\rho_b^2} \right) \nabla_a W_{ab} + \mathbf{g} \end{aligned} \quad (6)$$

where $r_{ab} = |\mathbf{r}_{ab}|$, $\mathbf{r}_{ab} = \mathbf{r}_a - \mathbf{r}_b$, $\mathbf{v}_{ab} = \mathbf{v}_a - \mathbf{v}_b$ and $\nabla_a W_{ab} = \nabla_a W(r_a - r_b, h)$. The second term on the right-hand side of Equation 4 is the delta-SPH (Molteni and Colagrossi, 2009) [60], which is diffusive and helps to reduce the numerical noise from the density fluctuations and to stabilize the pressure field. δ is a free parameter that needs to be attributed to a suitable value. However, $\delta = 0.1$ is recommended in DualSPHysics and works well for most applications (Crespo et al., 2015) [53]. The second term on the right-hand side of Equation 5 is the discrete form of the viscous stress (Lo and Shao, 2009), whereas the third term is the sub-particle scale (SPS) term, where τ is the SPS stress tensor (Dalrymple and Rogers, 2006) [43]. DualSPHysics also offers the artificial viscosity scheme proposed by Monaghan (1992) [57], which is a common method within fluid simulation using SPH due primarily to its simplicity. This scheme is not used in the current investigation.

2.1.3 Boundary Conditions

In DualSPHysics, the boundary is described by a set of particles that are considered as a separate set to the fluid particles. The software currently provides functionality for solid impermeable and periodic open boundaries. Methods to allow boundary particles to be moved according to fixed forcing functions are also available.

The Dynamic Boundary Condition (DBC) is the default method provided by DualSPHysics [Crespo et al., 2007] [50] to solid model boundaries. This method sees boundary particles that satisfy the same equations as fluid particles; however, their positions and velocities are not updated. Instead, they remain either fixed in position or move according to an imposed/assigned motion function (i.e. moving objects such as gates, wave-makers or floating objects). Using this boundary condition, when a fluid particle approaches a boundary particle, and the distance between them decreases beyond the kernel range, the density of the boundary particles increases, and giving rise to an increase in pressure. This results in a repulsive force being exerted on the fluid particle due to the pressure term in the momentum equation. This approach is not based on a rigorous

physical derivation and is known to suffer from accuracy issues. Nevertheless, this approach is easy to implement, computationally efficient, and naturally handles general 3-D shapes without knowing any geometric information about the boundary. This method's stability relies on the length of time step taken being suitably short to handle the highest present velocity of any fluid particles currently interacting with boundary particles. Therefore, it is an important point when considering how the variable time step is calculated. All the SPH simulations carried out in this work used this boundary condition to define the boundaries of the structure and the numerical tank.

Within DualSPHysics, it is possible to define a pre-imposed movement for a set of boundary particles. Various predefined movement functions are available, and the ability to assign a time-dependent input file containing kinematic detail. These boundary particles behave as a DBC described above; however, they move independently of the forces currently acting upon them rather than being fixed. This provides the ability to define complex simulation scenarios (i.e. a wave-making paddle) as the boundaries influence the fluid particles appropriately as they move.

2.1.4 Wave Modelling and Simulations

Piston-type long-crested wave generation schemes with second-order correction for long bound waves (sub-harmonics) available in DualSPHysics is used for generating both monochromatic (regular) and random waves. The numerical flume resembles a physical wave facility so that the moving boundaries mimic the action of a piston-type wavemaker (Altomare et al., 2017) [44].

A passive wave absorption technique available in DualSPHysics is used for generating a long time series of the waves in relatively short domains with negligible wave reflection. Passive wave absorbers are usually required to damp the wave energy and reduce reflection exerted by the model domain's boundary. A damping system is defined as a solution for passive absorption and is used to prevent wave reflection from fixed boundaries in the numerical flume (Altomare et al., 2017) [44]. The implemented absorption/damping system consists of gradually reducing the particles' velocity at each time step according to their location but using quadratic decay rather than exponential. This approach does not require a large region for the wave absorption; a length up to 1 wavelength is generally recommended.

2.2 Finite Volume Method (FVM)

In this study, a commercial general-purpose CFD software, Star-CCM+, was used, which offers solutions for various representations of the Navier-Stokes equations. In the present research, the FVM based modelling of wave-structure interaction was carried out using Reynolds-averaged Navier-Stokes (RANS) equations with a realizable k-ε two-layer turbulence model. The free surface was modelled using the Volume of Fluid (VOF) method, and a High-Resolution Interface Capturing (HRIC) scheme was activated. Detailed formulation

and equations of the applied numerical schemes can be found in the Star-CCM+ user manual.

2.3 Potential Flow Solutions (Boundary Element Method, BEM 2D)

A potential flow solution based on the Boundary Element Method (BEM) in 2D has been developed. The BEM formulation is summarized as follows. If fluid viscosity is neglected, the flow is irrotational, which guarantees the existence of a velocity potential function $\Phi(x, z, t)$, where x, z are the horizontal and vertical coordinates and t is time. We assume that this function is harmonic in time, i.e. $\Phi(x, z, t) = \phi(x, z)e^{-i\omega t}$ where ω is the frequency of the incident wave in rad/sec. The space-dependent velocity potential ϕ is the sum of the undisturbed potential ϕ_0 and the scattered potential ϕ_s . Since ϕ_0 is known from linear wave theory, we use the BEM to determine the scattered potential ϕ_s . The function ϕ_s satisfies Laplace's equation in the fluid domain, and this is converted to the following 2D boundary integral equation on the fluid boundary Γ .

$$\int_{\Gamma} \left([\phi_s - \phi_s(\vec{x}_p)] \frac{\partial \phi^*}{\partial n} - \phi^* \frac{\partial \phi_s}{\partial n} \right) d\Gamma \quad (7)$$

Here ϕ^* is the 2D fundamental solution

$$\phi^* = \frac{-1}{2\pi} \ln r$$

Where $r = |\vec{x} - \vec{x}_p|$, \vec{x} is the position vector of a general point in Γ and \vec{x}_p is the position vector of the source point in Γ . Equation 7 is discretized by a standard boundary element procedure and written as a linear combination of ϕ_s and its normal derivative $\frac{\partial \phi_s}{\partial n}$ on the boundary elements. The boundary conditions are as follows. On the mean free surface, we have the linearized condition:

$$\begin{aligned} \frac{\partial \phi_s}{\partial n} - \frac{\omega^2}{g} \phi_s &= 0 \quad \text{on the mean free surface} \\ \frac{\partial \phi_s}{\partial n} &= 0 \quad \text{on the sea bed (floor)} \\ \frac{\partial \phi_s}{\partial n} &= -\frac{\partial \phi_0}{\partial n} \quad \text{on the structure (Cylinder) surface} \\ \frac{\partial \phi_s}{\partial n} &= i\kappa \phi_s \quad (\kappa = \text{wave number}) \quad \text{on the radiation boundary} \end{aligned} \quad (8)$$

After ϕ_s is determined, the total (space-dependent) velocity potential is found as $\phi = \phi_0 + \phi_s$. The wave pressure is computed as $p = \rho \frac{\partial \Phi}{\partial t} = i\omega \rho \phi e^{-i\omega t}$ where ρ is the fluid density, and hence the wave forces on the cylinder can be found.

3. MODELLING AND VALIDATIONS

3.1 SPH Numerical Wave Tank

In the present SPH-based investigation, the Numerical Wave Tank (NWT) was modelled by performing wave

generation using piston-type second-order wave generation techniques (Medsen, 1971) [61] and the wave absorption/damping by a passive absorption technique. The second-order wave was created by making corrections of the first-order wave generation at the wavemaker by compensating both parasitic long waves and displacement long waves. The method implemented in DualSPHysics is based on the solution for the wavemaker's control signal that is described in (Barthel et al., 1993) [62]. The length of the wave absorption zone was close to one wavelength. In the present SPH NWT, the wave was generated immediately after the piston. However, the target wave was generated at the centre of the structure. All waves for the validation cases were completed in deep water conditions. The layout of the numerical wave tank with wave damping zone is presented in Figure 1.

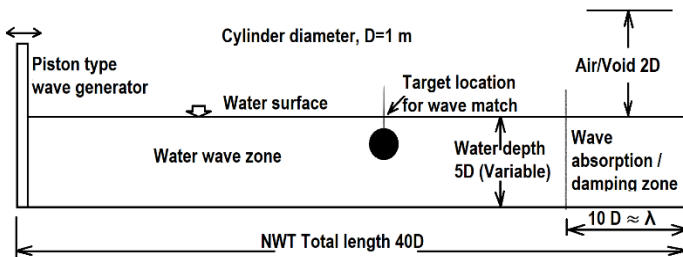


FIGURE 1: DEFINITION SKETCH OF THE NWT FOR MODELLING OF FREE SURFACE WAVES PAST A SUBMERGED HORIZONTAL CIRCULAR CYLINDER.

3.2 FVM Numerical Wave Tank

The NWT modelled in Star-CCM+ was as long as 9 wavelengths but very narrow for pseudo-2D application with symmetry conditions on sidewalls. The water depth varied to match the test condition. Also, the wave damping zone was created on the outlet pressure with 2 wavelengths. The wave damping coefficient was adjusted as following Peric's suggestion (Peric, 2015) [63]. A schematic of the FVM model domain is presented in Figure 2.

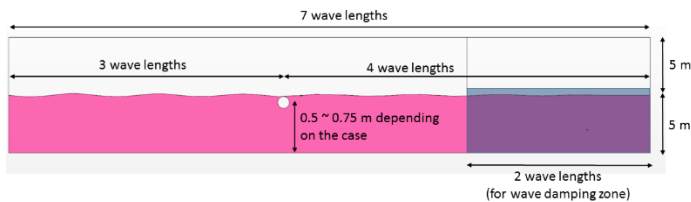


FIGURE 2: SCHEMATIC REPRESENTATION OF NUMERICAL DOMAIN FOR FVM BASED APPROACH

For incident waves, 5th order Stokes wave model was applied to consider the water depth effect properly. Five prismatic layers were attached to the structure and bottom. A fine mesh was generated around the free surface area based on 0.3% of wavelength and 3% of wave height, see Figure 3.

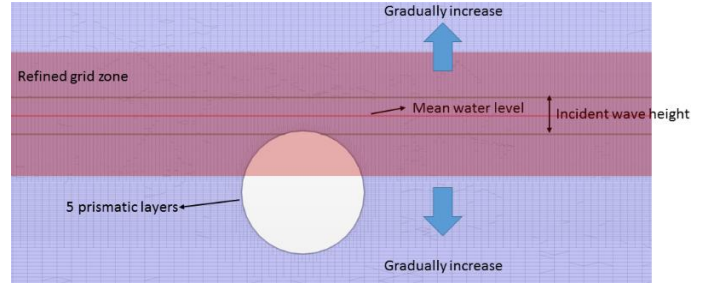


FIGURE 3: TYPICAL GRIDS FOR FVM BASED APPROACH.

3.2 Simulation Cases

Free surface waves past submerged horizontal circular and rectangular cylinders in different submergence depths and water depths were investigated numerically in the present study. The axis of the models was parallel to the wave crests. The definition sketch of free surface waves past a submerged horizontal circular cylinder is shown in Figure 4. Deep and transitional water waves were investigated for the circular cylinder case in the present study, where H_D is the water depth, a is the wave amplitude ($H_w=2a$, is wave height, 0.3 m), D is the cylinder diameter, d is the submergence depth, and λ is the wavelength ($\lambda=1.56 \cdot T^2$). The validation case involved a 1.0 m diameter circular cylinder and a rectangular cylinder of sides equal to 1.0 m, submerged in 5 m deep water and at varied submergence depths. Table 1 shows the circular cylinder's incident wave properties and corresponding submergence depth for the validation cases. The case setup refers to the experimental work by Khalil (2001) [26].

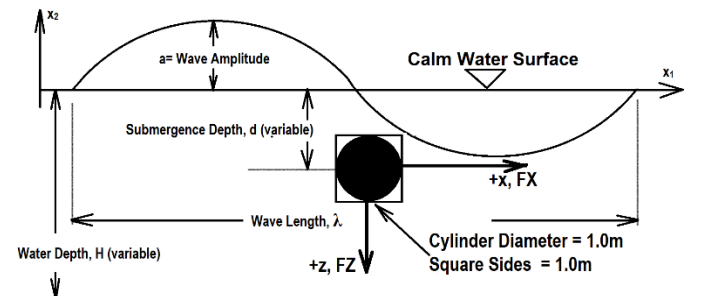


FIGURE 4: DEFINITION SKETCH OF THE FREE SURFACE WAVES PAST A CIRCULAR/SQUARE CYLINDER AND THE SIGN CONVENTIONS.

TABLE 1: SIMULATION CASES FOR THE MODEL VALIDATION AND SUBMERGENCE DEPTH EFFECT STUDY.

ID	d (m)	H_w (m)	T (sec)	λ (m)	$2d/D$	SPH	FVM	BEM
C1	0.5	0.3	2.244	7.86	1.00	X	X	-
C2	0.5625	0.3	2.244	7.86	1.125	X	X	-
C3*	0.625	0.3	2.244	7.86	1.25	X	X	-
C4	0.75	0.3	2.244	7.86	1.50	X	X	X
C5	1.0	0.3	2.244	7.86	2.00	X	-	X
C6	1.25	0.3	2.244	7.86	2.50	X	-	X
S1	0.5	0.3	2.244	7.86	1.00	X	-	-
S2	0.5625	0.3	2.244	7.86	1.125	X	-	-
S3	0.625	0.3	2.244	7.86	1.25	X	-	-
S4	0.75	0.3	2.244	7.86	1.50	X	-	-

3.3 SPH Convergence Study

The NWT was used to perform a wave force convergence study for the validation case C3 for regular waves. These cases are chosen for the particle size or inter-particle distance refinement study because this is the condition at which the maximum drift force and vertical force were recorded during the measurements. For this case, the NWT was $40 D$ long and $10 D$ high with a still water depth of $5 D$. For Case 1, the submerged cylinder was placed at $20 D$ horizontally away from the wave generator piston and its top surface was touching the calm water surface. Table 2 and Figure 5 summarized the results of the convergence study and comparison with the corresponding measurements from Khalil (2001) [26] in terms of normalized force components. Figure 6 shows the particle size refinement study in terms of surface elevation, which was recorded at the center of the structure (20 m downstream of the wave piston, approximately 3 times the wavelength), without it being present. The wave elevation obtained from the linear wave theory or dispersion relation is included for comparison purposes. Based on the results, the inter-particle distance of 0.01 m was deemed sufficient and used for the remainder of the simulations.

TABLE 2: PARTICLE RESOLUTION CONVERGENCE STUDY FOR THE MODEL VALIDATION.

Particles (Millions)	Particle Size (mm)	FX'_SPH	FX'_Khalil_2001	FZ'_SPH	FZ'_Khalil_2001
0.1	0.05	0.031	-0.053	-2.036	-0.227
0.5	0.02	-0.065	-0.053	-0.730	-0.227
1.9	0.01	-0.060	-0.053	-0.257	-0.227
3.4	0.0075	-0.057	-0.053	-0.232	-0.227
7.6	0.005	-0.055	-0.053	-0.238	-0.227

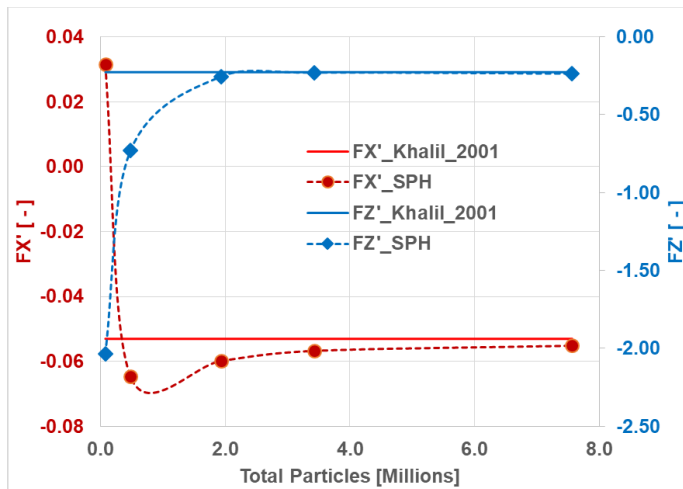


FIGURE 5: PARTICLE RESOLUTION CONVERGENCE FOR COMPARISON OF SPH PREDICTIONS OF CYLINDER FORCES WITH MEASUREMENTS.

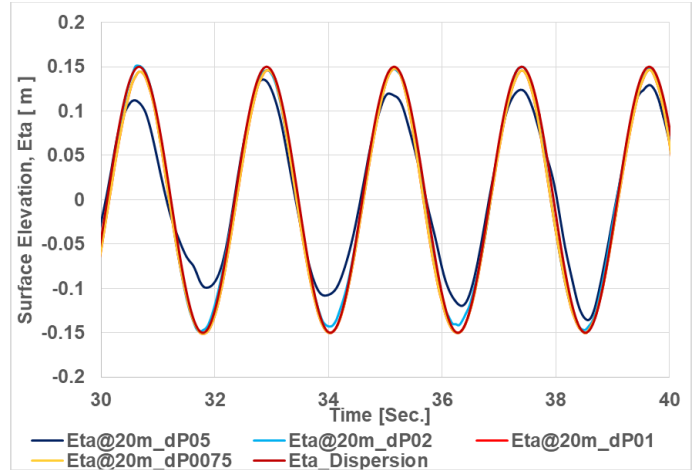


FIGURE 6: PARTICLE RESOLUTION CONVERGENCE OF SPH PREDICTED WATER SURFACE ELEVATION.

3.3 FVM Convergence Study

A brief grid dependency study was carried out for the FVM model in Star-CCM+ for the C3 case. The base mesh size wave varied between 0.3 mm to 0.10 mm, and 0.15 mm was judged as sufficient for the simulations. Time step size was set to 0.5% of the wave period. However, the applied time step and the grid size may not be sufficient to capture the wave impact and small droplets when the wave breaking occurs, but it is expected to be small enough to simulate the wave drift force from the grid dependency test. A summary results of the grid sensitivity study is presented in Figure 7.

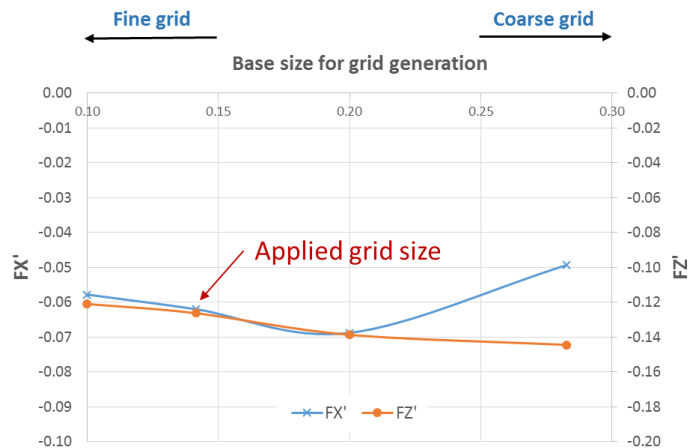


FIGURE 7: GRID CONVERGENCE FOR NON-DIMENSIONAL DRIFT FORCE USING FVM BASED APPROACH (C3).

3.4 Comparison of Numerical Predictions and Measurements

Figure 8 and Figure 9 present the summary of the predicted and measured normalized time-averaged mean horizontal forces, acting on the circular cylinder and the rectangular cylinder, respectively, at various depths of submergences. The normalized force component is presented in the figure, which also shows the normalization formulation used. Both the SPH predictions and

measurements show a highly nonlinear variation of the normalized force as the structure is submerged from the top of the surface, touching the calm water surface to nearly 0.25D submergence. The FVM (Star-CCM+) also captured the nonlinear trend and provided a reasonable comparison considering the numerical approaches used. The measurements and the predictions showed close to zero drifting force when the normalized submergence distance, $2d/D \geq 2.0$.

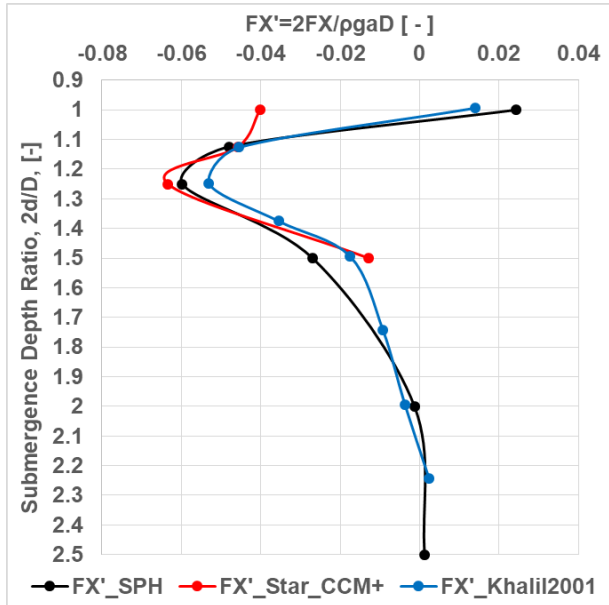


FIGURE 8: COMPARISON OF MEAN HORIZONTAL FORCE ON THE CIRCULAR CYLINDER IN THE WAVE BETWEEN THE SPH AND CFD PREDICTED AND KHALIL 2001 MEASUREMENTS.

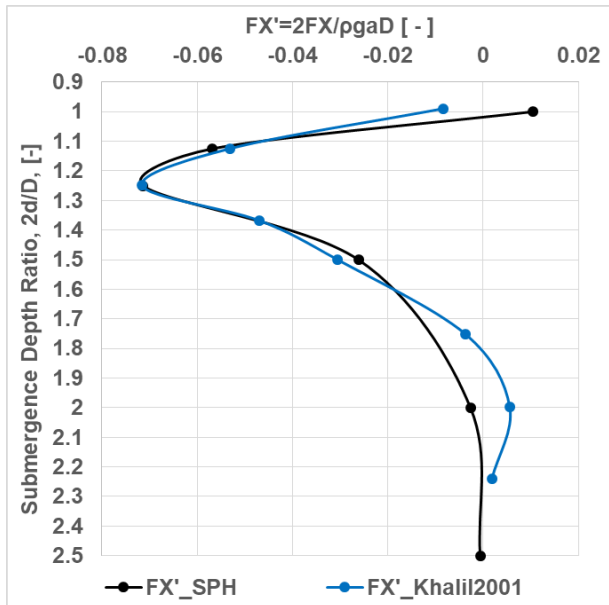


FIGURE 9: COMPARISON OF MEAN HORIZONTAL FORCE ON THE RECTANGULAR CYLINDER IN THE WAVE BETWEEN THE SPH PREDICTED AND KHALIL 2001 MEASUREMENTS.

The vertical force curves exhibit approximately similar characteristics; see Figure 10 and Figure 11 for the circular cylinder and the rectangular cylinder, respectively.

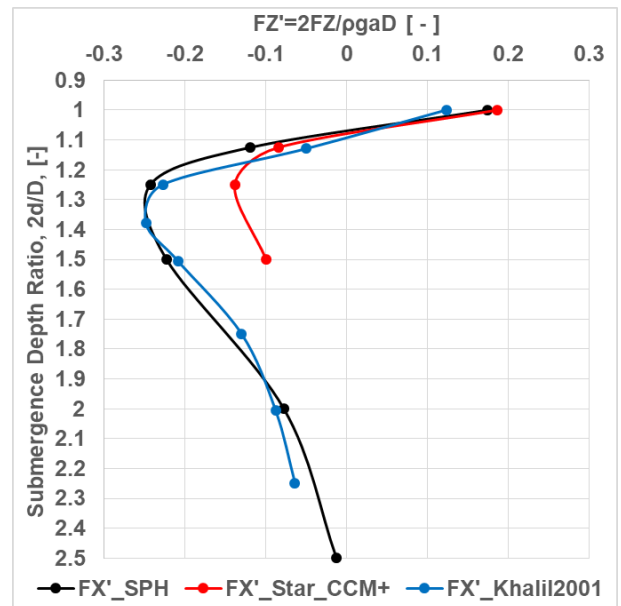


FIGURE 10: COMPARISON OF MEAN VERTICAL FORCE ON THE CIRCULAR CYLINDER IN THE WAVE BETWEEN THE SPH AND CFD PREDICTED AND KHALIL 2001 MEASUREMENTS.

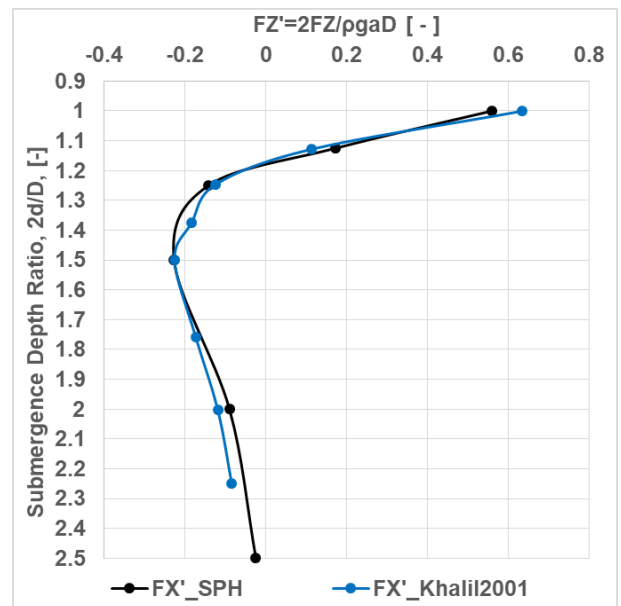


FIGURE 11: COMPARISON OF MEAN VERTICAL FORCE ON THE RECTANGULAR CYLINDER IN THE WAVE BETWEEN THE SPH PREDICTED AND KHALIL 2001 MEASUREMENTS.

4. RESULTS AND DISCUSSIONS

4.1 Submergence Depth Effect on Wave Forces

Further to the results presented in Figure 8 through Figure 11, both the measurements and SPH predictions show that the

maximum negative drifting forces on the rectangular cylinder were greater than on the circular cylinder. Thus, the SPH model confirmed that the nonlinear effect was less severe in the circular than the rectangular cylinder. The general trend of variation of the horizontal drift forces due to the change of submergence depth is that the negative drift force steadily increases with the decreasing submergence depth and then abruptly decreases when a part of the structure emerges above the free water surface. The horizontal drift forces tend to vanish when the normalized submergence depth, $2d/D$, becomes greater than 2.0. The general trend of variation of the vertical forces due to the change of submergence depth is that the upward mean force steadily increases with the decreasing submergence depth and then abruptly decreases when a part of the structure emerges above the free water surface. The upward forces tend to vanish when the normalized submergence depth, $2d/D$, becomes greater than 2.0. Overall, the SPH-based model well captured the nonlinear trends of both force curves.

Figure 12 and Figure 13 presents the time series of the horizontal and vertical forces, respectively, on the circular cylinder at different submergence depths. The raw data predicted by the SPH model is filtered at 1 Hz in these figures. Since the wave generated was close to pure sinusoidal waves (deep water wave), the predicted forces should also show sinusoidal fluctuations when the model is deeply submerged (wave not disturbed by the structure's presence). However, the record of both horizontal and vertical forces in the shallowly submerged condition shows very peaky wave profiles, which are simply the manifestation of nonlinear wave effects. The nonlinear effect is absent in the case of deeply submerged cases irrespective of their shapes. As the depth of submergence decreases, a negative drifting force is developed on both structures. This negative drift force (upwave force, Khalil 2001) attains a peak value around $2d/D=1.25$. These trends were also observed during the measurements, as mentioned in Khalil (2001) [26]. These nonlinear effects are shown more clearly in the zoomed-in data, as presented in Figure 14 and Figure 15, which presents the normalized horizontal and vertical forces for five wave-loading cycles.

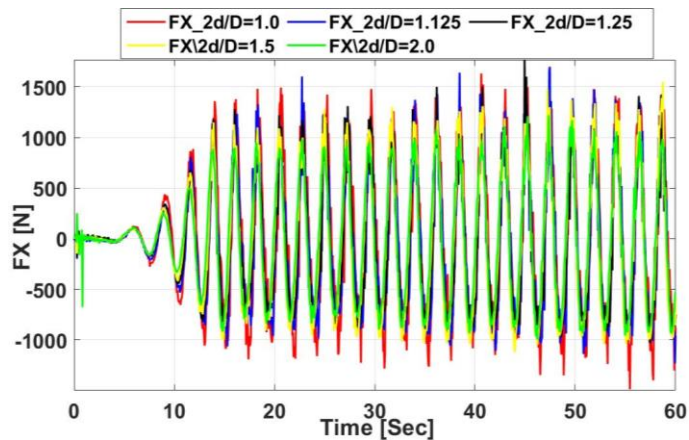


FIGURE 12: SPH MODEL PREDICTED HORIZONTAL FORCE TIME SERIES ON THE CIRCULAR CYLINDER IN THE C CASES.

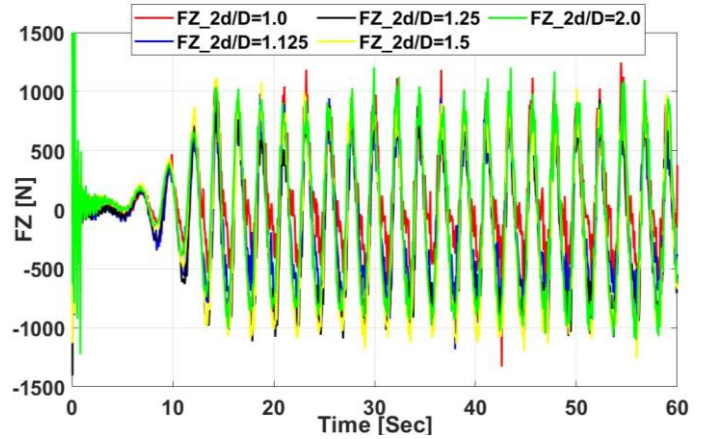


FIGURE 13: SPH MODEL PREDICTED VERTICAL FORCE TIME SERIES ON THE CIRCULAR CYLINDER IN THE C CASES.

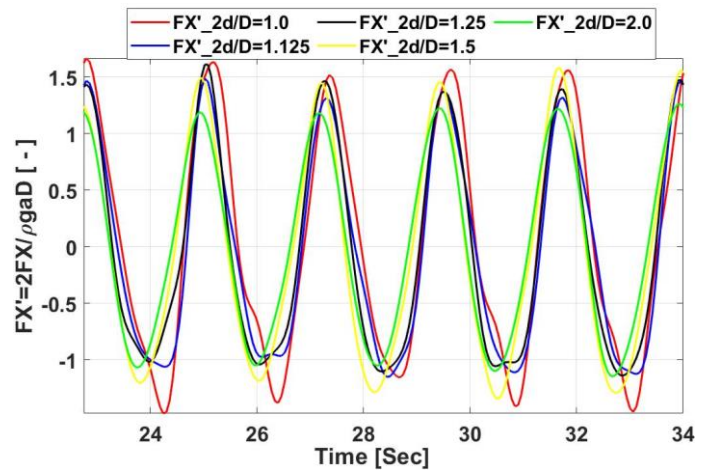


FIGURE 14: SPH MODEL PREDICTED NORMALIZED HORIZONTAL FORCE TIME SERIES ON THE CIRCULAR CYLINDER FOR FIVE LOADING CYCLES.

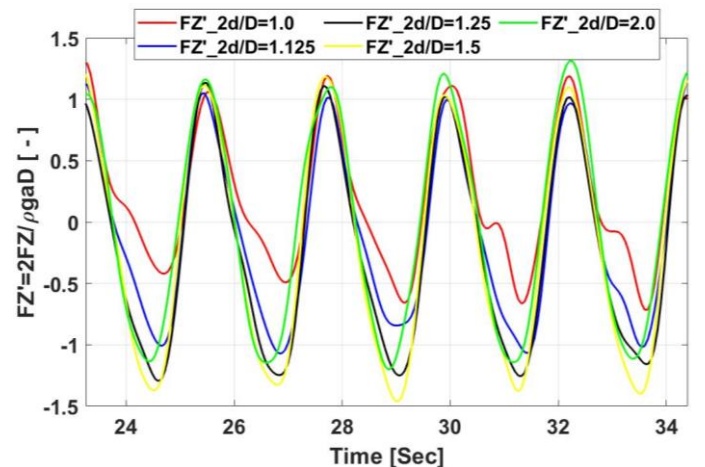


FIGURE 15: SPH MODEL PREDICTED NORMALIZED VERTICAL FORCE TIME SERIES ON THE CIRCULAR CYLINDER FOR FIVE LOADING CYCLES.

Figure 16 and Figure 17 show the iso-surface of the velocity distribution of the wavefield at two distinct stages of the wave-cylinder interaction at a submergence depth of $2d/D=1.0$. The three stages are, firstly, at 33.6 seconds of the simulation when the wave peak nearest to the upstream side of the cylinder center was approximately 2 m away, and secondly, at 34.2 seconds when the wave peak was at the cylinder center. Figure 18, through Figure 23, show the velocity distribution of the wavefield at the same instances at other submergence depths as mentioned in each figure title. Figures 24 through 27 shows similar velocity distributions for the rectangular cylinder at 1.25 and 1.5 submergence depths.

In the current simulation, both structures remained completely submerged under the wave action when $2d/D$ exceeds 1.3, or the top of the structure is 0.15 m below the free water surface. The top of both structures pierces the free water surface, and a part of it is exposed to air when $2d/D < 1.3$. This means at the $2d/D$ of 1.0, 1.125 or 1.25, the top of the structures pierce the water surface and thereby induces strong nonlinear interactions with the incident waves. As the submergence depth further increases, this negative drifting force rapidly decreases, see Figures 8 through 11. This negative force is a direct consequence of the nonlinear interaction of the waves with the top surface of the cylinder; as the wave passes over the shallowly submerged cylinder and then breaks behind it. The wave-breaking behind the cylinder results in the formation of vortices which are evident in the SPH predictions, and they disappear as the cylinder submerged below $2d/D$ of 1.5.

Overall, the SPH model well-captured the geometric effect of shallowly submerged cylinders and confirmed that the geometry plays a vital role in the wave-structure interactions. Generally, the negative horizontal drift force acting on a rectangular cylinder was predicted greater than on a circular cylinder. It is only the horizontal component of the static pressure acting on the rear side of the circular model, which contributes to the negative drifting force. On the other hand, the entire static pressure acting normal to the flat vertical rear side of the rectangular model is responsible for the large upwave force. The larger vertical force on the rectangular cylinder for the shallowly submerged condition is primarily due to the larger and flat exposed surface.

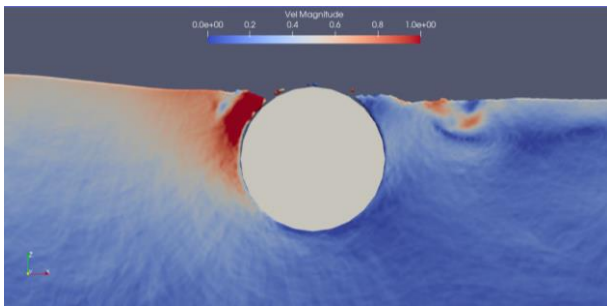


FIGURE 16: VELOCITY DISTRIBUTION OF THE FLOW-FIELD AROUND THE CIRCULAR CYLINDER: SUBMERGENCE DEPTH 1.0 (d/D), SIMULATION TIME 33.6 SECONDS.

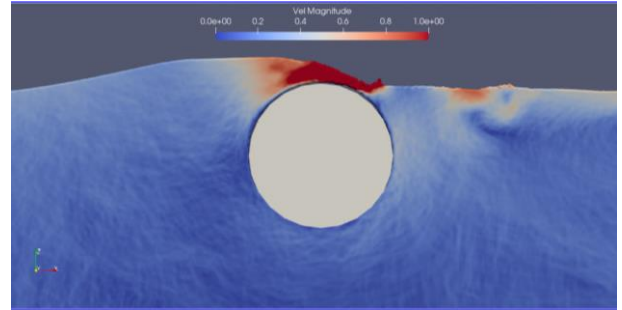


FIGURE 17: VELOCITY DISTRIBUTION OF THE FLOW-FIELD AROUND THE CIRCULAR CYLINDER: SUBMERGENCE DEPTH 1.0 (d/D), SIMULATION TIME 34.2 SECONDS.

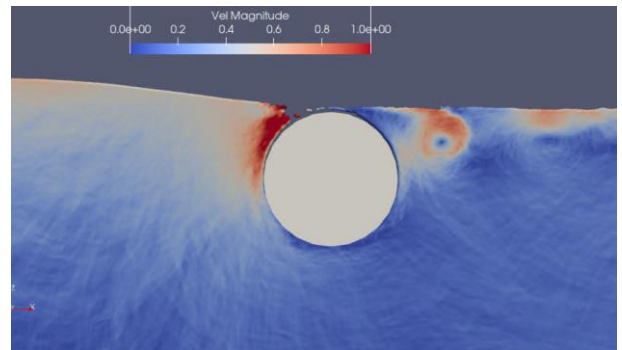


FIGURE 18: VELOCITY DISTRIBUTION OF THE FLOW-FIELD AROUND THE CIRCULAR CYLINDER: SUBMERGENCE DEPTH 1.25 (d/D), SIMULATION TIME 33.6 SECONDS.

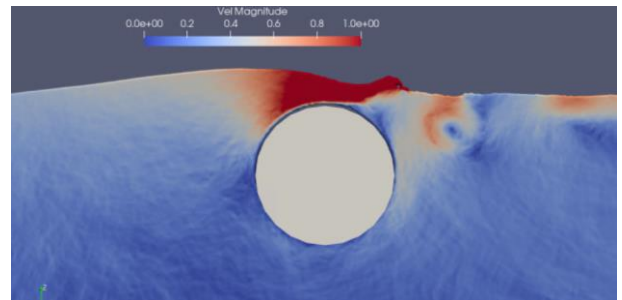


FIGURE 19: VELOCITY DISTRIBUTION OF THE FLOW-FIELD AROUND THE CIRCULAR CYLINDER: SUBMERGENCE DEPTH 1.25 (d/D), SIMULATION TIME 34.2 SECOND.

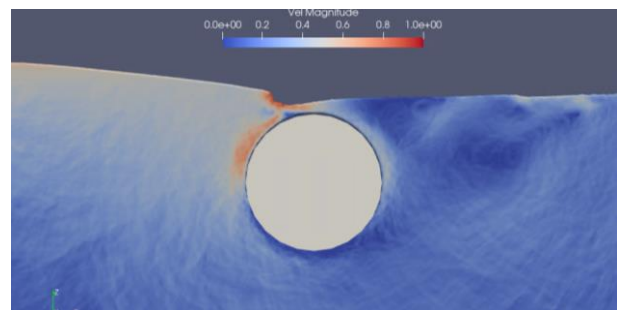


FIGURE 20: VELOCITY DISTRIBUTION OF THE FLOW-FIELD AROUND THE CIRCULAR CYLINDER: SUBMERGENCE DEPTH 1.5 (d/D), SIMULATION TIME 33.6 SECONDS.

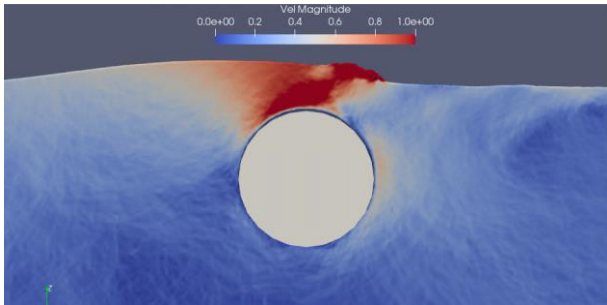


FIGURE 21: VELOCITY DISTRIBUTION OF THE FLOW-FIELD AROUND THE CIRCULAR CYLINDER: SUBMERGENCE DEPTH 1.5 (d/D), SIMULATION TIME 34.2 SECOND.

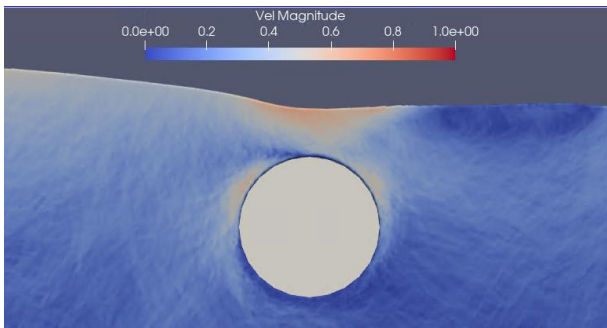


FIGURE 22: VELOCITY DISTRIBUTION OF THE FLOW-FIELD AROUND THE CIRCULAR CYLINDER: SUBMERGENCE DEPTH 2.0 (d/D), SIMULATION TIME 33.6 SECOND.

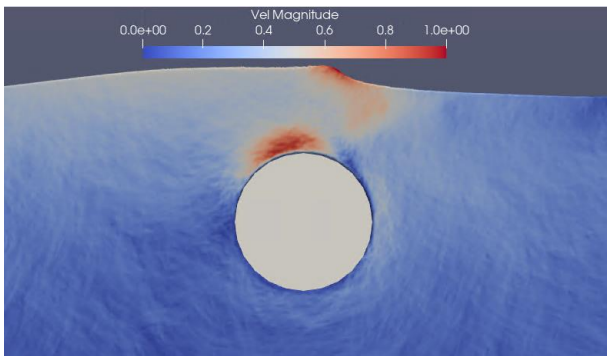


FIGURE 23: VELOCITY DISTRIBUTION OF THE FLOW-FIELD AROUND THE CIRCULAR CYLINDER: SUBMERGENCE DEPTH 2.0 (d/D), SIMULATION TIME 34.2 SECOND.

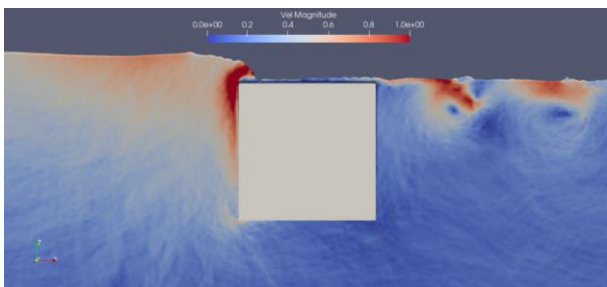


FIGURE 24: VELOCITY DISTRIBUTION OF THE FLOW-FIELD AROUND THE RECTANGULAR CYLINDER: SUBMERGENCE DEPTH 1.25 ($2d/D$), SIMULATION TIME 27.0 SECOND.

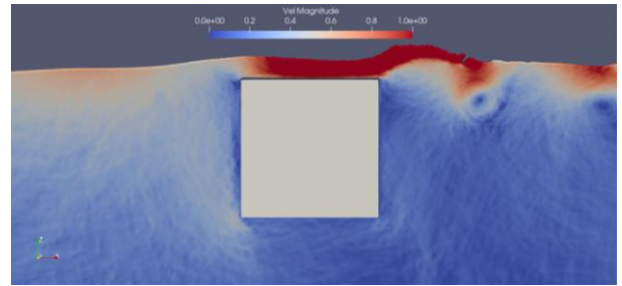


FIGURE 25: VELOCITY DISTRIBUTION OF THE FLOW-FIELD AROUND THE RECTANGULAR CYLINDER: SUBMERGENCE DEPTH 1.25 ($2d/D$), SIMULATION TIME 27.9 SECOND.

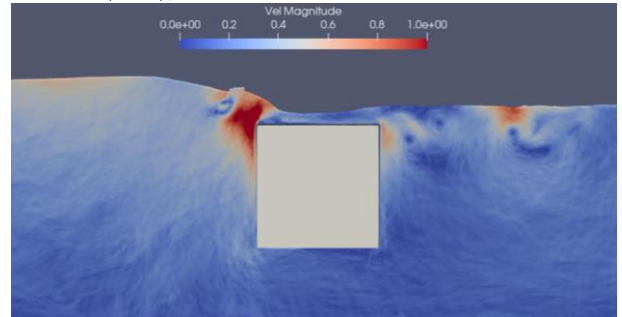


FIGURE 26: VELOCITY DISTRIBUTION OF THE FLOW-FIELD AROUND THE RECTANGULAR CYLINDER: SUBMERGENCE DEPTH 1.5 ($2d/D$), SIMULATION TIME 27.0 SECOND.

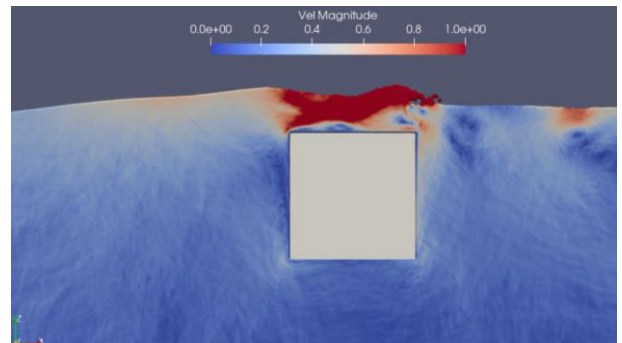


FIGURE 27: VELOCITY DISTRIBUTION OF THE FLOW-FIELD AROUND THE RECTANGULAR CYLINDER: SUBMERGENCE DEPTH 1.5 ($2d/D$), SIMULATION TIME 27.6 SECOND.

The BEM model cannot capture nonlinear wave-structure interactions for the shallowly submerged cylinder as nonlinear effects from wave breaking and higher-order components were not modelled. However, BEM can predict the cyclic wave forces in the horizontal and vertical directions when the cylinder remained completely submerged. Figures 28 and 29 present a comparison between SPH and BEM model predictions of the average of the force amplitudes in the horizontal and vertical directions, respectively, due to change in the submergence depths. It is clear from the figures that the BEM can be suitable to estimate the changes in wave force amplitude due to the submerged depth.

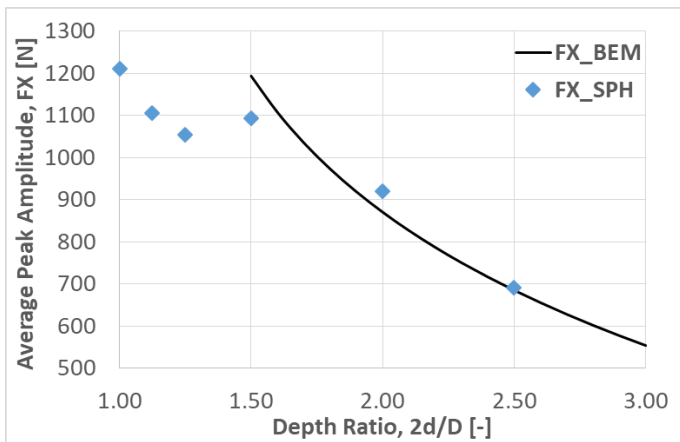


FIGURE 28: PREDICTION OF THE EFFECT OF SUBMERGENCE DEPTH ON THE AVERAGE AMPLITUDE OF THE HORIZONTAL WAVE FORCE.

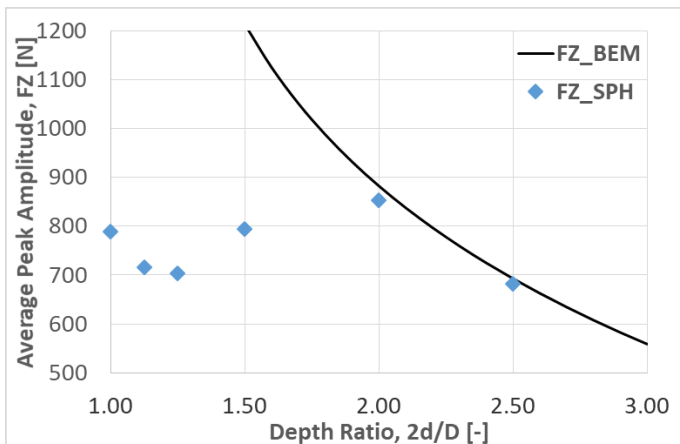


FIGURE 29: PREDICTION OF THE EFFECT OF SUBMERGENCE DEPTH ON THE AVERAGE AMPLITUDE OF THE VERTICAL WAVE FORCE.

The numerical model presented in this paper is two-dimensional. The results can be applied directly for cylinders in long-crested seas, but for long cylinders, in short-crested seas, the cylinder should be studied in full 3D. Since the end conditions become significant, the results do not apply to very small aspect ratios (cylinder length/diameter). Significant scattering or diffraction is not expected for a cylinder diameter of 1 m and wavelength of ~8 m. Further study should be carried out to investigate the SPH capabilities in modelling the nonlinear wave-structure interactions for a larger structure where the wave diffraction becomes dominant.

5. CONCLUSION

In the current work, we have used a Smoothed Particle Hydrodynamics (SPH)-based tool to investigate the nonlinear interactions between large waves and submerged horizontal structures, one circular and one rectangular, at various submergence depths deep water conditions. We applied a Finite Volume Method (FVM) and a Boundary Element Method (BEM)

based tools to limited analysis cases for comparison study with other existing numerical models. Through this work, we validated an SPH-based model to predict the wave-structure interaction forces, especially time-averaged drift components, in deep water regular waves. An extensive literature survey of various existing tools and techniques to predict the wave interactions with submerged structures is provided for completeness.

The nonlinear wave forces predicted by the SPH and FVM were attributed to breaking waves behind a shallowly submerged cylinder. The negative drifting force in shallowly submerged cases is attributed to a direct consequence of wave-breaking. Therefore this drifting force tends to vanish when the cylinder is deeply submerged. The SPH and CFD modellings were able to capture the breaking of waves around a shallowly submerged structure and simulate nonlinear wave drift forces in the horizontal and vertical directions.

The numerical model presented in this paper is two-dimensional. The results can be applied directly for cylinders in long-crested seas, but for long cylinders, in short-crested seas, the cylinder should be studied in full 3D. The results do not apply to very small aspect ratios (cylinder length/diameter) since the end conditions then become significant. Significant scattering or diffraction is not expected for a cylinder diameter of 1 m and wavelength of ~8m. Further study should be carried out to investigate the SPH capabilities in modelling the nonlinear wave-structure interactions for a larger structure where the wave diffraction becomes dominant. We plan to investigate larger and more extreme shallow, transitional and deep water regular and irregular waves interacting with large structures.

ACKNOWLEDGEMENTS

The authors are indebted to the National Research Council's Ocean Coastal and River Engineering Research Center for supporting this numerical modelling endeavour.

REFERENCES

- [1] Moonesun M, Ghasemzadeh F, Korol Y, et al. Effective depth of regular wave on submerged submarines and AUVs. *Int Rob Auto J.* 2017;2(6):208-216. DOI: 10.15406/iratj.2017.02.00037
- [2] Dean, WR (1948). "On the Reflexion of Surface Waves by a Submerged Circular Cylinder," *Proc Camb Phil Soc*, Vol 44, pp 483-491.
- [3] Ursell, F (1949). "Surface Waves in the Presence of a Submerged Circular Cylinder, I and II," *Proc Camb Phil Soc*, Vol 46, pp 141-158.
- [4] Ogilvie, TF (1963). "First- and Second-Order Forces on a Cylinder Submerged Under a Free Surface," *J Fluid Mech*, Vol 16, pp 451-472.
- [5] Vada, T., 1987, A numerical solution of the second-order wave-diffraction problem for a submerged cylinder of arbitrary shape, *Journal of Fluid Mechanics*, 174, 23-37.
- [6] Wu, GX (1993). "Hydrodynamic Forces on a Submerged Circular Cylinder Undergoing Large-amplitude Motion," *J Fluid Mech*, Vol 254, pp 41-58.

- [7] Skotner, C., Jonsson, I.G., Skourup, J., 1994, Wave forces on a large, horizontal submerged cylinder, *Ocean Engineering*, Volume 21, Issue 8, 1994, Pages 711-731, ISSN 0029-8018, [https://doi.org/10.1016/0029-8018\(94\)90048-5](https://doi.org/10.1016/0029-8018(94)90048-5).
- [8] Teixeira, P. 2010, Numerical simulation of the interaction of a regular wave and a submerged cylinder, 2010 Third Southern Conference on Computational Modeling, 978-0-7695-3976-8/09, DOI 10.1109/MCSUL.2009.13.
- [9] Guerber, E., Benoit, M., Grilli, S.T., Buvat, C., 2010. Modelling of fully nonlinear wave interactions with moving submerged structures. In: Proceedings of the 20th International Offshore and Polar Engineering Conference (ISOPE), Beijing, China, pp.529–536.
- [10] Guerber, E., Benoit, M., Grilli, S.T. and Buvat, C., 2012. A fully nonlinear implicit model for wave interactions with submerged structures in forced or free motion, *Engineering Analysis with Boundary Elements*, 36(7), 1151–1163.
- [11] Koh, H.-J., Cho, I.-H., 2011, computation of the inviscid drift force caused by nonlinear waves on a submerged circular cylinder, *International Journal of Naval Architecture and Ocean Engineering*, Volume 3, Issue 3, 2011, Pages 201-207, ISSN 2092-6782, <https://doi.org/10.2478/IJNAOE-2013-0063>.
- [12] Bai, W., Hannan, M.A. and Ang, K.K., 2014. Numerical simulation of fully nonlinear wave interaction with submerged structures: Fixed or subjected to constrained motion, *Journal of Fluids and Structures*, 49(8), 534–553.
- [13] Chen, Z.M., 2012. A vortex-based panel method for potential flow simulation around a hydrofoil. *Journal of Fluids and Structures* 28, 378–391.
- [14] Kim, J.R.; Koh, H.J.; Ruy, W.S.; Cho, I.H. Experimental study on the hydrodynamic behaviours of two concentric cylinders. In Proceedings of the 2013 World Congress on Advances in Structural Engineering and Mechanics (ASEM13), Jeju, Korea, 8–12 September 2013.
- [15] Morison, J. R.; O'Brien, M. P.; Johnson, J. W.; Schaaf, S. A. (1950), "The force exerted by surface waves on piles", *Petroleum Transactions, American Institute of Mining Engineers*, 189: 149–154, doi:10.2118/950149-G.
- [16] Dixon, A., Salter, S., & Greated, C. (1979). Wave Forces on Partially Submerged Cylinders. *Journal of the Waterway, Port, Coastal and Ocean Division*, 105, 421-438.
- [17] Chaplin, J.R., 1981. On the irrotational flow around a horizontal cylinder in waves, *Journal of Applied Mechanics*, 48(4), 689–694.
- [18] Chaplin, J.R., 1984a. Mass transport around a horizontal cylinder beneath waves, *Journal of Fluid Mechanics*, 140, 175–187.
- [19] Chaplin, J.R., 1984b. Nonlinear forces on a horizontal cylinder beneath waves, *Journal of Fluid Mechanics*, 147, 449–464.
- [20] Chaplin, J.R., 2001. Nonlinear wave interactions with a submerged horizontal cylinder, Proceedings of the 11th International Offshore and Polar Engineering Conference, ISOPE, Stavanger, Norway, Vol. 3, pp. 272–279.
- [21] Contento, G. and Codiglia, R., 2001. Nonlinear free surface-induced pressure on a submerged horizontal circular cylinder at low Keulegan-Carpenters numbers, *Applied Ocean Research*, 23(3), 175–185.
- [22] Tavassoli, A. and Kim, M.H., 2001. Interactions of fully nonlinear waves with submerged bodies by a 2D viscous NWT, Proceedings of the 11th International Offshore and Polar Engineering Conference, ISOPE, Stavanger, Norway, Vol. 3, pp. 348–354.
- [23] Longuet-Higgins, M.S., 1977. The mean forces exerted by waves on floating or submerged bodies with applications to sand bars and wave power machines, *Proceedings of the Royal Society. Series A, Mathematical and Physical Sciences*, 352(1671), 463–480.
- [24] Inoue, R. and Y. Kyojuka. "On the nonlinear wave forces acting on submerged cylinders." *Journal of the Society of Naval Architects of Japan* 1984 (1984): 115-127.
- [25] Schonberg T and Chaplin J R (2003) Computation of Nonlinear Wave Reflections and Transmissions from Submerged Horizontal Cylinder, *Int. J. Offshore and Polar Eng.* j. 13: 29-37.
- [26] Khalil, G., 2001, Experimental investigation of wave forces on submerged horizontal cylinders, *Indian Journal of Engineering and Material Sciences*, Vol. 8, April 2001, pp. 59-65.
- [27] Conde, J.M.P., Didier, E., Lope, M.F.P., Gato, L.M.C., 2009. Nonlinear wave diffraction by a submerged horizontal circular cylinder. *International Journal of Offshore and Polar Engineering* 19, 198–205.
- [28] Muellenhoff, W., Slotta, L., "Investigation of the forces on a submerged cylinder due to surface water waves," *IEEE 1971 Conference on Engineering in the Ocean Environment*, San Diego, CA, USA, 1971, pp. 58-63, doi: 10.1109/OCEANS.1971.1161053.
- [29] Violeau, D., Rogers, B.D., 2016. Smoothed particle hydrodynamics (SPH) for free-surface flows: past, present and future. *Journals of Hydraulic Research*. 54 (1), 1–26.
- [30] Xiao, H., Huang, W., Liu, C., 2013, Numerical modelling of wave-current forces acting on a horizontal cylinder of marine structures by VOF method, June 2013, *Ocean Engineering* 67:58-67, DOI: 10.1016/j.oceaneng.2013.01.027
- [31] Ottens, H., Pistidda, A., and van Dijk, R., 2014. "Cfd analysis of waves over a submerged cylinder in close proximity of the free surface". In ASME 2014 33rd International Conference on Ocean, Offshore and Arctic Engineering, San Francisco, America. American Society of Mechanical Engineers.
- [32] Chen, B., Lu, L., Greated, C., Kang, H., Investigation of wave forces on partially submerged horizontal cylinders by numerical simulation, *Ocean Engineering* 107(2015)23–31.
- [33] Liu, S., Ong, M. C., Obhrai, C., and Seng, S. (December 6, 2017). "Computational Fluid Dynamics Simulations of Regular and Irregular Waves Past a Horizontal Semi-Submerged Cylinder." *ASME. J. Offshore Mech. Arct. Eng.* June 2018; 140(3): 031801. <https://doi.org/10.1115/1.4038349>.
- [34] Teng, B., Mao, H.F. & Lu, L. Viscous Effects on Wave Forces on A Submerged Horizontal Circular Cylinder. *China Ocean Eng* 32, 245–255 (2018). <https://doi.org/10.1007/s13344-018-0026-9>.

- [35] Aristodemo, F., Tripepi, G., Meringolo, D.-D., Veltri, P., 2017, Solitary wave-induced forces on horizontal circular cylinders: Laboratory experiments and SPH simulations, *Coastal Engineering*, Volume 129, 2017, Pages 17-35, ISSN 0378-3839, <https://doi.org/10.1016/j.coastaleng.2017.08.011>.
- [36] Zhong, Z., Wang, K.H., 2009, Modeling fully nonlinear shallow-water waves and their interactions with cylindrical structures, *Computers & Fluids*, Volume 38, Issue 5, 2009, Pages 1018-1025, ISSN 0045-7930, <https://doi.org/10.1016/j.compfluid.2008.01.032>.
- [37] Delorme, L., Colagrossi, A., Souto-Iglesias, A., Zamora-Rodríguez, R., Botía-Vera, E., 2009. A set of canonical problems in sloshing, Part I: pressure field in forced roll comparison between experimental results and SPH. *Ocean. Eng.* 36 (2), 168–178.
- [38] Sun, P., Ming, F., Zhang, A., 2015. Numerical simulation of interactions between the free surface and rigid body using a robust SPH method. *Ocean. Eng.* 98, 32–49.
- [39] Pugliese Carratelli, E., Viccione, G., Bovolín, V., 2016. Free surface flow impact on a vertical wall: a numerical assessment. *Theor. Comp. Fluid Dyn.* 30 (5), 403–414.
- [40] Aristodemo, F., Federico, I., Veltri, P., Panizzo, A., 2010. Two-phase SPH modelling of advective-diffusion processes. *Environ. Fluid Mech.* 10, 451–470.
- [41] Federico, I., Marrone, S., Colagrossi, A., Aristodemo, F., Antuono, M., 2012. Simulating 2D open-channel flows through an SPH model. *Eur. J. Mech. B/Fluids* 34, 35–46.
- [42] Aristodemo, F., Marrone, S., Federico, I., 2015. SPH modelling of plane jets into water bodies through an inflow/outflow algorithm. *Ocean. Eng.* 105, 160–175.
- [43] Dalrymple, R., Rogers, B., 2006, Numerical modelling of water waves with SPH method, *Coastal Engineering*, Vol 53, No 2-3, pp 141-147, 2006.
- [44] Altomare, C., Domínguez, J.M., Crespo, A.J.C., Gonz_alez-Cao, J., Suzuki, T., 2017, Long-crested wave generation and absorption for SPH-based DualSPHysics model, *Coastal Engineering* 127 (2017) 37–54.
- [45] Altomare, C., Crespo, A.J.C., Domínguez, J.M., G_omez-Gesteira, M., Suzuki, T., Verwaest, T., 2015. Applicability of Smoothed Particle Hydrodynamics for estimation of sea wave impact on coastal structures. *Coast. Eng.* 96, 1–12.
- [46] Meringolo, D.D., Aristodemo, F., Veltri, P., 2015. SPH numerical modelling of wave perforated breakwater interaction. *Coast. Eng.* 101, 48–68.
- [47] Ren, B., Wen, H., Dong, P., Wang, Y., 2014. Numerical simulation of wave interaction with porous structures using an improved smoothed particle hydrodynamic method. *Coast. Eng.* 88, 88–100.
- [48] Bouscasse, B., Colagrossi, A., Marrone, S., Antuono, M., 2013. Nonlinear water wave interaction with floating bodies in SPH. *J. Fluids Struct.* 42, 112–129.
- [49] Barreiro, A., Crespo, A.J.C., Domínguez, J.M., García-Feal, O., Zabala, I., G_omez-Gesteira, M., 2016. Quasi-Static Mooring solver implemented in SPH. *J. Ocean Eng. Mar. Energy* 2 (3), 381–396.
- [50] Crespo, A.J.C., Altomare, C., Domínguez, J.M., Gonz_alez-Cao, J., G_omez-Gesteira, M., 2017. Towards simulating floating offshore oscillating water column converters with Smoothed Particle Hydrodynamics. *Coast. Eng.* 126, 11–26.
- [51] Marrone, S., Colagrossi, A., Antuono, M., Colicchio, G., Graziani, G., 2013. An accurate SPH modelling of viscous flow around bodies at low and moderate Reynolds numbers. *J. Comp. Phys.* 245, 456–475.
- [52] Bouscasse, B., Colagrossi, A., Marrone, S., Souto-Iglesias, A., 2017. SPH modelling of viscous flows past a circular cylinder interacting with a free surface. *Comput. Fluids* 146, 190–212.
- [53] Crespo, A.J.C.; Domínguez, J.M.; Rogers, B.D.; Gómez-Gesteira, M.; Longshaw, S.; Canelas, R.; García-Feal, O. DualSPHysics: Open-Source Parallel CFD Solver Based on Smoothed Particle Hydrodynamics (SPH). *Comput. Phys. Commun.* 2015, 187, 204–216.
- [54] Wendland H. Piecewise polynomial, positive definite and compactly supported radial functions of minimal degree. *Advance Computational Mathematics*, 1995; 4: 389–96. <https://doi.org/10.1007/BF02123482>.
- [55] Monaghan JJ. 1994. Simulating free surface flows with SPH. *Journal of Computational Physics*, 110, 399–406.
- [56] Monaghan JJ. Cas, RAF, Kos AM, Hallworth M, 1999. Gravity currents descending a ramp in a stratified tank. *Journal of Fluid Mechanics*, 379, 39–70.
- [57] Monaghan JJ. 1992. Smoothed particle hydrodynamics. *Annual Review of Astronomy and Astrophysics*, 30, 543- 574.
- [58] Mohaghan, J., 2012, Smoothed Particle Hydrodynamics and Its Diverse Applications, *Annual Review of Fluid Mechanics*, Vol 44, pp 323-346, 2012.
- [59] Liu, M., Liu, G., 2010, Smoothed Particle Hydrodynamics (SPH): an Overview and Recent Developments”, *Archives of Computational Methods in Engineering*, Vol. 17, no.1, pp 25-76, 2010.
- [60] Molteni, D., Colagrossi, A., 2009, A Simple procedure to improve the pressure evaluation in hydrodynamic context using the SPH, *Computer Physics Communications*, Vol 180, No. 6, 861-872, 2009.
- [61] Madsen, O. S., 1971. On the generation of long waves. *J. Geophys. Res.* 76, 8672–8673.
- [62] Barthel FC, Mansard V, Sand P, Vis SE. 1983. Group bounded long waves in physical models. *Ocean Engineering*, 10, 261–294.
- [63] Peric, R., and Moustafa, A-M. (2015). Reliable Damping of Free Surface Waves in Numerical Simulations. *Ship Technology Research.* 63. 10.1080/09377255.2015.1119921.